ELSEVIER

Journal of Alloys and Compounds 320 (2001) 302–307

Journal of ALLOYS AND COMPOUNDS

www.elsevier.com/locate/jallcom

Coupled thermodynamic/kinetic analysis of diffusional transformations during laser hardening and laser welding

G.N. Haidemenopoulos*

Department of Mechanical and Industrial Engineering, University of Thessaly, GR-38334, Volos, Greece

Abstract

Several important industrial material processes, such as welding and surface treatments with high energy beams, incorporate rapid thermal cycles characterized by high heating/cooling rates and short dwell times. Computational simulation of the evolution of microstructure under these extreme conditions has received rather limited attention. With the advent of modern computational tools regarding alloy thermodynamics and kinetics, it is possible to simulate the progress of diffusional phase transformations and thus to predict microstructural development. In the present work, moving boundary diffusion problems have been simulated for two cases. In the first case the rapid austenitization during laser transformation hardening of a hypoeutectoid steel was examined. The effects of heating rate, maximum temperature, dwell time and initial microstructure fineness were analyzed. In the second case the aging, dissolution and coarsening of strengthening precipitates in the heat affected zone of laser welds in Al–Mg–Si alloys was examined. The simulation provided the variation of the volume fraction and average size of the strengthening phase during the weld thermal cycle. In both cases the calculations were performed by applying the coupled thermodynamics and kinetics approach, incorporated in the DICTRA program. This kind of simulation provides useful information for the design of the above processes.

Keywords: Rapid austenitization; Computational thermodynamics; Kinetics; Dissolution; Coarsening; Weld thermal cycle

1. Introduction

Laser transformation hardening and laser welding are both novel processes, which incorporate a moving high-energy laser beam to treat industrial alloys. Both processes induce a very rapid thermal cycle on the material with heating rates of the order of 10^4°C/s and accordingly short dwell times and high cooling rates. In the case of laser transformation hardening of steels this thermal cycle induces rapid austenitization of a surface layer followed by martensitic transformation. The resulting hardening depends among other factors on the extent of austenitization, which in turn depends on processing parameters (e.g. laser beam power and travel speed). Therefore, the simulation of austenite formation during rapid heating can provide insight to the effect of processing parameters on microstructure formation and can lead to an efficient design of the laser transformation hardening process. In the case of welding of aluminium alloys the rapid thermal cycle induces rapid melting and solidification of the weld pool as well as several solid state transformations in the heat affected zone (HAZ), such as coarsening and dissolution of the strengthening phases. These transformations degrade the strength of the HAZ and limit the application of welding as a joining technique in age-hardenable aluminium alloys. Laser welding compared to conventional welding, results in a significantly narrower weld pool and HAZ with associated reductions in thermal stresses and distortions. However, the problem of material degradation in the HAZ remains. Again, the simulation of microstructural evolution of the HAZ undergoing a rapid thermal cycle can assist the design of the laser welding process.

A reliable simulation of diffusional transformations is one that combines both thermodynamic and kinetic calculations. Computational thermodynamics is based on the CALPHAD method [1–4]. According to this method thermodynamic models are used for the description of the Gibbs free energy of phases as a function of temperature, composition and pressure. The model parameter values are obtained from experimental thermodynamic data through an optimization procedure. Computational kinetics on the other hand is based on the numerical solution of the multicomponent diffusion equations in a microstructural domain under specific boundary and initial conditions. The DICTRA method [5] combines an explicit description of

*Tel.: +30-42-174-062; fax: +30-42-174-061.
E-mail address: hgreg@mie.uth.gr (G.N. Haidemenopoulos).

0925-8388/01/$ – see front matter
PII: S0925-8388(00)01493-6

the diffusion equations with thermodynamic calculations assuming local thermodynamic equilibrium at the moving interface. The diffusion flux of a species is related to the chemical potential gradient rather than the concentration gradient, while mobilities are used instead of diffusivities so that the thermodynamic driving forces and couplings between diffusing elements are taken into account. The DICTRA program is linked to Thermo-Calc [6] for the calculation of the local equilibrium at the interphase boundaries.

The present paper describes initial results of the above methodology in the cases of laser hardening of steels [7] and laser welding of aluminium alloys [8].

2. Rapid austenitization during laser transformation hardening

Laser transformation hardening is a novel surface hardening process, which incorporates a CO_2 laser beam for rapid heating of the steel surface. The steel is austenitized and subsequently self-quenched to form martensite. The size and microstructure of the HAZ as well as the resulting hardness profiles depend on the transient temperature distribution imposed on the material which is a function of process parameters such as laser power, laser beam diameter and laser travel speed [9,10]. The material is subjected to a rapid thermal cycle characterized by a very high heating rate of the order of 10^4°C/s, a short dwell time (above the A_1 temperature) of the order of few milliseconds and an accordingly high cooling rate, sufficient to form martensite in hypoeutectoid steels. The steel under consideration is the Ck-60 steel with chemical composition 0.6 wt% C, 0.75 wt% Mn and with A_1 and A_3 temperatures 727 and 751°C respectively. The first step towards the simulation of rapid austenitization is the calculation of the temperature distribution in the HAZ and the associated thermal cycles. The heat flow calculations were performed with the finite element method, employing the ABAQUS software package. Typical results of the calculations are shown in Fig. 1 for laser power 1500 W, laser beam diameter 5 mm and laser travel speed of 3 m/min. The thermal cycle is depicted for four nodes under the laser beam at varying depths below the surface (z=0, 0.1, 0.3 and 0.5 mm). The peak temperature is reached in about 0.1 s while the heating rate decreases with the depth below the surface. The dwell time depends also on the depth and ranges between 20 and 50 ms. The next step in the simulation is the set up of the geometrical model for the numerical solution of the diffusion equations. The starting microstructure in Ck-60 steel consists of proeutectoid ferrite and pearlite. According to previous work of Speich et al. [11] austenitization takes place in two discrete steps. At first the pearlite dissolves to form austenite. When pearlite dissolution is completed, further austenitization proceeds with the transformation of proeutectoid ferrite to

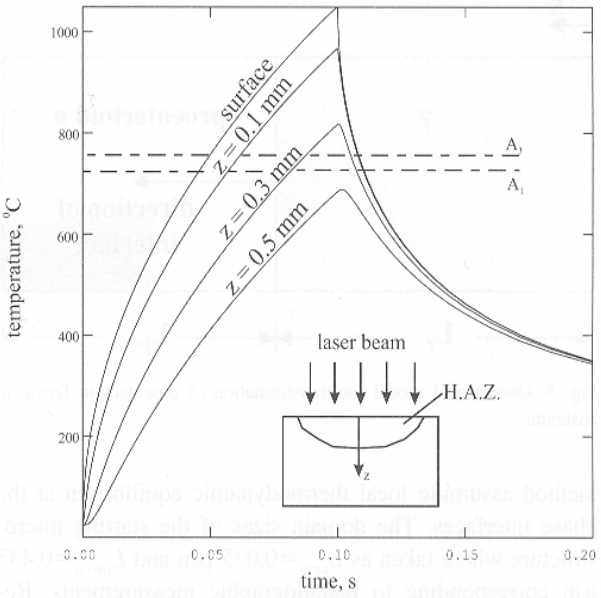

Fig. 1. Thermal cycles at various depths below the surface of laser treated Ck-60 steel.

austenite. Therefore, two geometrical models have been constructed in order to simulate the two austenitization steps. Fig. 2a depicts the geometrical representation of pearlite as alternating lamellae of ferrite and cementite with half-lengths L_{ferr} and L_{cem}, respectively. The dashed line depicts the calculation domain. Austenite nucleation is considered to take place heterogeneously in the ferrite/cementite interfaces as depicted in Fig. 2b. The model domain of the second austenitization step is shown in Fig. 3 where austenite is growing at the expense of proeutectoid ferrite. The simulations were carried out with the DICTRA

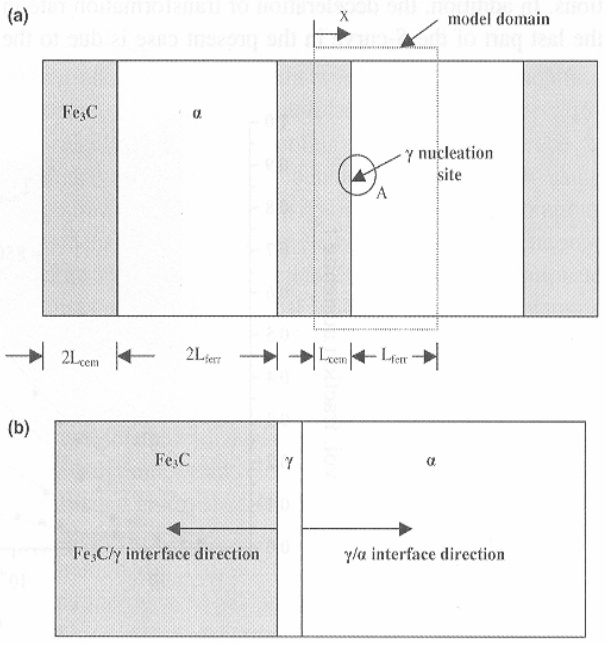

Fig. 2. Geometrical model for pearlite dissolution. (a) Model domain, (b) magnification of area A showing movement of interphase boundaries.

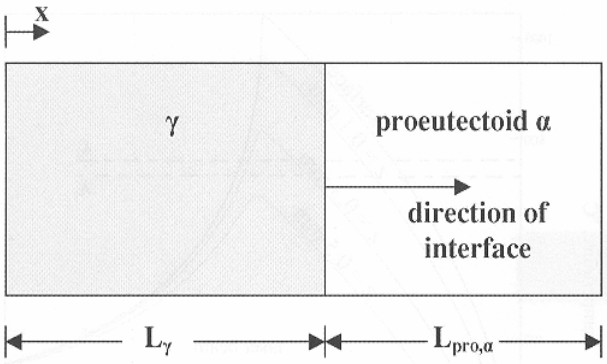

Fig. 3. Geometrical model for transformation of proeutectoid ferrite to austenite.

method assuming local thermodynamic equilibrium at the phase interfaces. The domain sizes of the starting microstructure where taken as L_{cem}=0.025 μm and $L_{pro,a}$=0.433 μm corresponding to metallographic measurements. Results of the simulation are shown in Fig. 4, which depicts the volume fraction of austenite, f_γ, as a function of dwell time τ for maximum temperatures of 750, 800, 850 and 900°C. The points correspond to the results of the simulation, while the lines are the best fit of the equation

$$f_\gamma = 1 - \exp(-k\tau^n) \quad (1)$$

where k and n are constants. The value of exponent n is close to 0.5 in all simulations. Eq. (1) is of an Avrami-like type, yielding the well known sigmoidal vol. fraction–time curve. However, there are significant differences between Eq. (1) and the Avrami equation. In the present study, a non-isothermal heat treatment is considered, whereas the Avrami approach regards isothermal phase transformations. In addition, the deceleration of transformation rate in the last part of the S-curve in the present case is due to the significantly slower rate of austenitization, during the dissolution of proeutectoid ferrite. In contrast, the corresponding decrease of transformation rate in the Avrami analysis is due to the hard impingement of the growing phase regions.

The results of Fig. 4 show that for T_{max}=750 and 800°C austenitization is not completed within the available dwell time. Fig. 5 depicts the volume fraction of austenite formed as a function of depth below the surface. It is apparent that complete austenitization has occurred only at a depth of 0.2 mm while the austenite volume fraction becomes zero at a depth of 0.6 mm. Assuming that all the austenite formed during rapid heating transforms to martensite on cooling, it is obvious that there will be a variation of martensite content (and thus hardness) in the HAZ. It is obvious that the simulation can assist in the selection of the process parameters in order to reach the desirable hardening effect.

3. Dissolution and coarsening in the HAZ of aluminium laser welds

Laser welding imposes a rapid thermal cycle in the HAZ. Taking the 6000 series alloys as an example, depending on the initial age condition (0, T6 or other), solid state reactions such as precipitation, coarsening or dissolution of the strengthening phase may take place in the HAZ during heating or even cooling. Fig. 6 shows an isopleth of the Al–Mg–Si system at Si=0.74 wt%. For the 6061-T6 alloy (0.98 wt% Mg, 0.74 wt% Si) one can identify three temperature regions with respect to changes in the HAZ. Above the aging temperature, coarsening of stable and metastable precipitates takes place. Between 400°C and the equilibrium solvus temperature, coarsening of stable and dissolution of metastable precipitates occurs

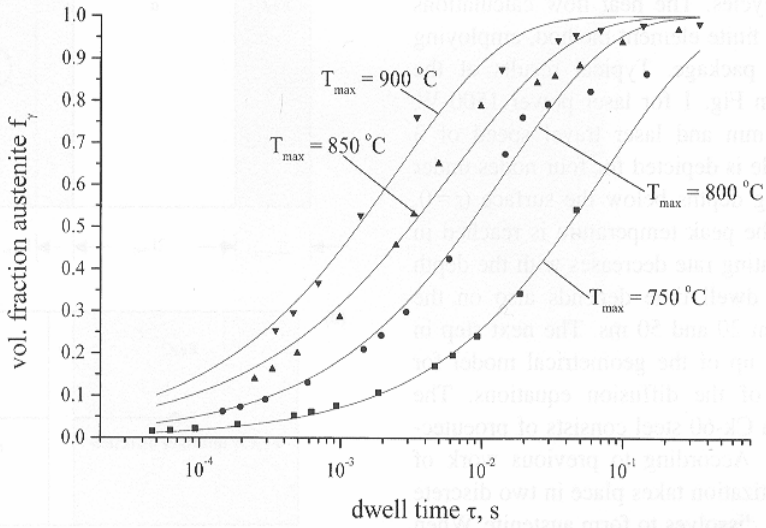

Fig. 4. Variation of austenite volume fraction as a function of dwell time for various maximum temperatures of the thermal cycle. Full lines correspond to a best fit of the Avrami equation.

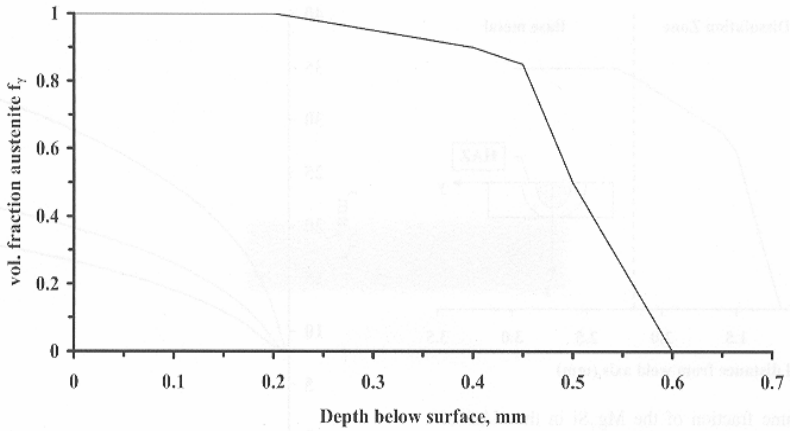

Fig. 5. Austenite volume fraction as a function of depth below the surface in the HAZ of laser-treated Ck-60 steel.

in the HAZ. Above the equilibrium solvus boundary the stable precipitates dissolve. As in the previous example, the simulation starts by calculating the temperature distribution and the thermal cycle in the HAZ. These calculations have been performed by employing the finite element package ABAQUS, using a three-dimensional mesh. Typical results of the calculations are shown in Fig. 7 for laser power 3 kW, laser beam diameter 1 mm and laser travel speed 9 m/min. The thermal cycle is depicted at three nodes in the HAZ for $y=1.2$, 1.22 and 1.25 mm all at a depth of $z=0.5$ mm. The thermal cycles are characterized by extremely large heating and cooling rates as well as very short dwell times. The geometrical model used for the simulation of the dissolution of Mg_2Si (β) precipitates is shown in Fig. 8. Since the β precipitates are rod-like, a

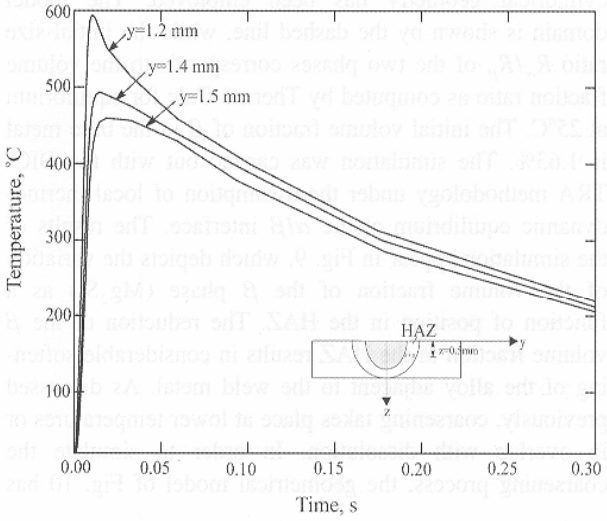

Fig. 7. Thermal cycles at various lateral positions in the heat affected zone at a depth of 0.5 mm below the surface.

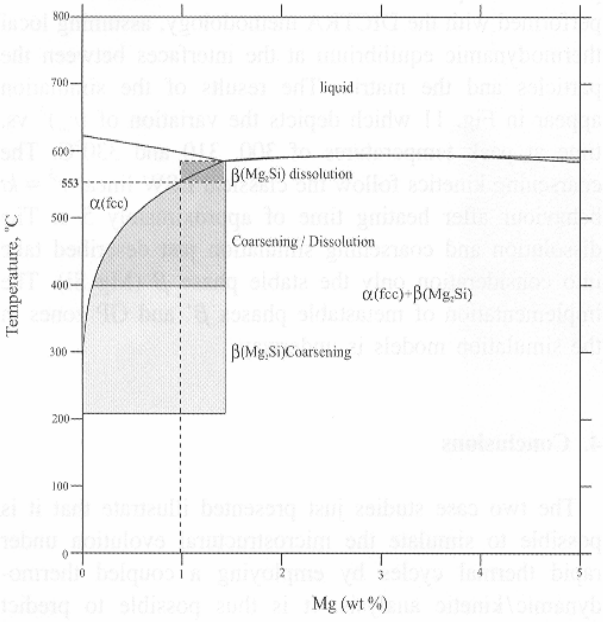

Fig. 6. Isopleth of the Al–Mg–Si phase diagram at Si=0.74 wt% showing temperature regimes for coarsening and dissolution of strengthening precipitates during welding.

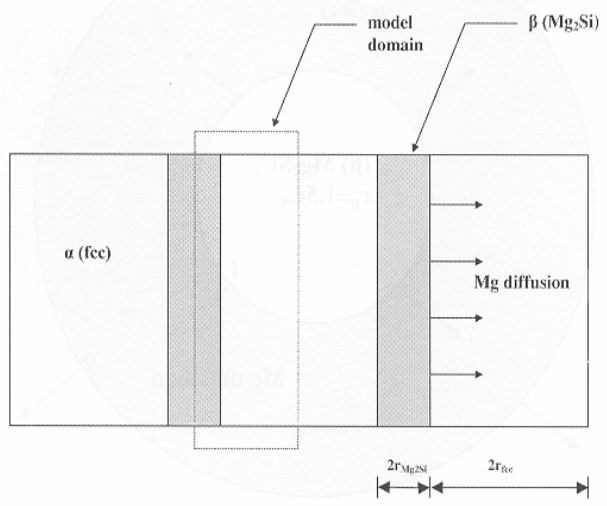

Fig. 8. Geometrical model for the dissolution of Mg_2Si precipitates in the HAZ of laser welds. The dashed line shows the model domain.

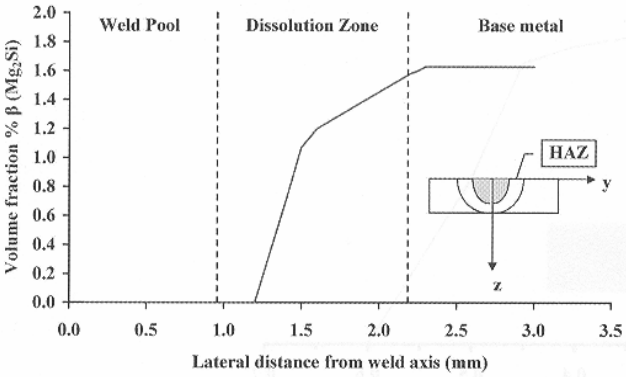

Fig. 9. Variation of the volume fraction of the Mg_2Si in the HAZ of a laser weld as predicted by the simulation of the dissolution during the weld thermal cycle.

cylindrical geometry has been employed. The model domain is shown by the dashed line, while the initial size ratio R_α/R_β of the two phases corresponds to the volume fraction ratio as computed by Thermo-Calc for equilibrium at 25°C. The initial volume fraction of β in the base metal is 1.63%. The simulation was carried out with the DICTRA methodology under the assumption of local thermodynamic equilibrium at the α/β interface. The results of the simulation appear in Fig. 9, which depicts the variation of the volume fraction of the β phase (Mg_2Si) as a function of position in the HAZ. The reduction of the β volume fraction in the HAZ results in considerable softening of the alloy adjacent to the weld metal. As discussed previously, coarsening takes place at lower temperatures or in overlap with dissolution. In order to simulate the coarsening process, the geometrical model of Fig. 10 has

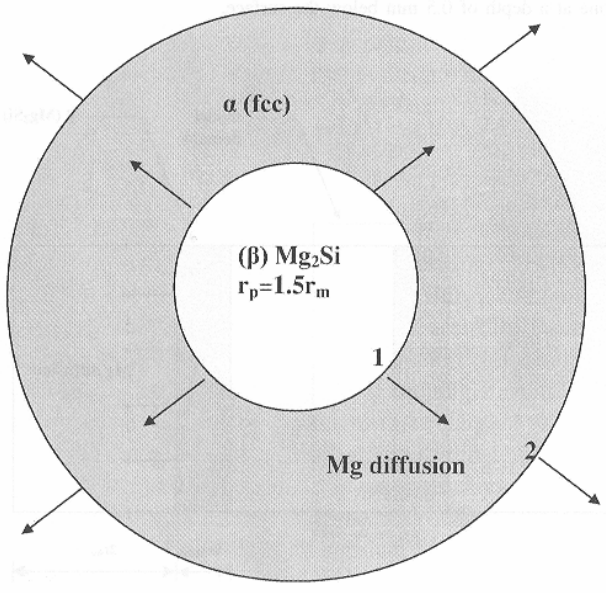

Fig. 10. Geometrical model for the simulation of the coarsening of Mg_2Si precipitates in the HAZ.

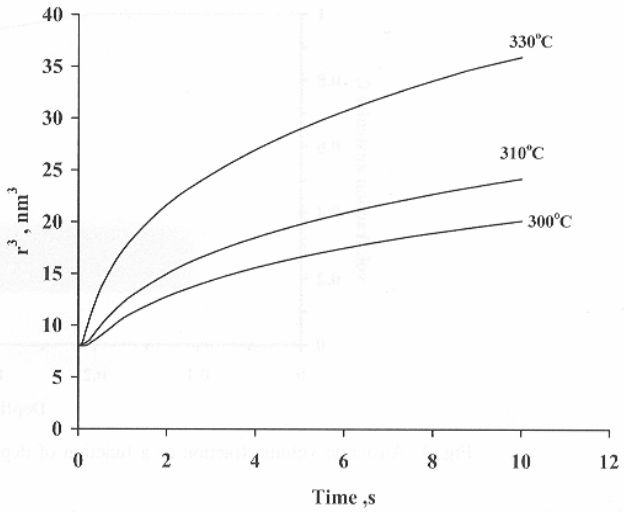

Fig. 11. Variation of the average radius of Mg_2Si precipitates as a function of time at peak temperature of the thermal cycle showing that coarsening kinetics follow the classical LSW behavior after 5 s.

been constructed using spherical geometry for the particle dispersion. In accordance with the LSW theory of coarsening [12,13] a particle with radius $r_p = 1.5r_m$ (r_m being the average particle radius) is growing under a concentration gradient in the matrix of α(FCC) controlled by the terminal concentrations at the interfaces (points 1 and 2 in Fig. 10). These concentrations follow a Gibbs–Thomson dependence on particle radius. Since the diffusivity of Mg in Al is much lower than the diffusivity of Si in Al it has been considered that coarsening is controlled by the diffusion of Mg only. The initial phase sizes correspond to the ratio of the volume fraction of α(FCC) and $\beta(Mg_2Si)$ phases in equilibrium at 25°C. The calculations were performed with the DICTRA methodology, assuming local thermodynamic equilibrium at the interfaces between the particles and the matrix. The results of the simulation appear in Fig. 11 which depicts the variation of $(r_m)^3$ vs. time at peak temperatures of 300, 310 and 330°C. The coarsening kinetics follow the classical LSW linear $r^3 = kt$ behaviour after heating time of approximately 5 s. The dissolution and coarsening simulation just described take into consideration only the stable phase β (Mg_2Si). The implementation of metastable phases β' and GP zones in the simulation models is underway.

4. Conclusions

The two case studies just presented illustrate that it is possible to simulate the microstructural evolution under rapid thermal cycles by employing a coupled thermodynamic/kinetic analysis. It is thus possible to predict quantitatively the effects of heating or cooling rates as well as dwell time on microstructural features which control properties such as hardness or yield strength. The direct

link between process parameters and properties show that these simulations can be a very powerful tool for alloy design and process optimization.

References

[1] L. Kaufman, H. Bernstein, Calculation of Phase Diagrams, Academic Press, New York, 1970.
[2] L. Kaufman, CALPHAD 1 (1977) 1.
[3] H.L. Lukas, J. Weiss, E.T. Henig, CALPHAD 6 (1982) 229–251.
[4] J. Agren, Curr. Opin. Solid State Mater. Sci. 1 (1996) 355–360.
[5] J. Agren, ISIJ Int. 32 (1992) 291.
[6] B. Sundman, B. Jansson, J.-O. Anderson, CALPHAD 9 (1985) 153–190.
[7] A.I. Katsamas, Laser Transformation Hardening and Laser Carburizing of Low Alloy Steels, Doctoral Thesis Research in progress, Dept. Mechanical and Industrial Engineering, University of Thessaly, Greece, 2000.
[8] A. Zervaki, Microstructural Evolution in the HAZ of Laser Welds in Age-Hardenable Aluminium Alloys, Doctoral Thesis Research in progress, Dept. Mechanical and Industrial Engineering, University of Thessaly, Greece, 2000.
[9] A.I. Katsamas, A.D. Zervaki, G.N. Haidemenopoulos, Steel Res. 68 (1997) 119–124.
[10] A.I. Katsamas, G.N. Haidemenopoulos, Surf. Coat. Technol. 115 (1999) 249–255.
[11] G.R. Speich, V.A. Demarest, R.L. Miller, Metall. Trans. A 12A (1981) 1419–1428.
[12] I.M. Lifshitz, V.V. Slyozov, J. Phys. Chem. Solids 19 (1961) 35.
[13] C. Wagner, Z. Electrochem. 65 (1961) 581.